





Practical and Numerical Investigation on a Minimal Design Navigation System of Bats

Yasufumi Yamada¹ , Kentaro Ito², Ryo Kobayashi^{3,4}, Shizuko Hiryu^{1,5} ,
and Yoshiaki Watanabe¹

¹ Doshisha University, Kyotanabe, 610-0321, Japan
yasufumi.yamada1@gmail.com

² Hosei University, Koganei, 184-0002, Japan

³ Hiroshima University, Higashi-Hiroshima, 739-8526, Japan

⁴ JST CREST, Chiyodaku, Tokyo, 102-0076, Japan

⁵ JST PRESTO, Chiyodaku, Tokyo, 102-0076, Japan

Abstract. In this study, to investigate how the behavioral strategy employed by bats contributed to acoustic navigation based on a minimal design sensing, we conducted vehicle experiments and numerical simulation based on a simple algorithm inspired by bats. Especially, a double-pulse scanning method was proposed as a bat-inspired navigation algorithm in which (1) the direction of pulse emission was alternately shifted between the direction of movement and the direction of the nearest obstacle, and (2) the direction of movement was calculated for every double-pulse emission based on integrated information from all echoes detected by double-pulse sensing. To quantify that method, a conventional scanning method was also developed. The conventional scanning method was that (1) the pulse direction was fixed in the direction of travel of the car body and (2) the moving direction was calculated for every pulse emission. As a result of 100 repeated drives with autonomous vehicle equipped with 1 transmitter and 2 receivers in a practical course, the success rate of an obstacle-avoidance drive on a test course improved from 13% for conventional method to 73% with the proposed method. Furthermore, the numerical simulation demonstrated that the proposed method operate the robust path planning by suppressing the localization ambiguity due to interference of multiple echoes. These practical experiments and numerical simulation suggest that bats employed the simple behavioral solution on the operation of acoustic sensing for various problems occurring in the real world.

Keywords: Awareness in distributed, ambient, and pervasive environments
Echolocation · Bats · Autonomous vehicle · Bio-inspired-navigation

1 Introduction

Echolocating bats perceive spatial information using ultrasonic sensing even in the absence of visual information. They emit ultrasound pulses from the nose or mouth and detect the returning echoes with the right and left ears, which can be regarded as the minimum sensor requirement for three-dimensional (3D) spatial sensing. From the view

point of sensor inputs, echolocation acquires a one-dimensional time-amplitude signals, but since visual sensing acquires two-dimensional images, the raw sensor inputs of echolocation seem to be fewer than those of visual sensing. Nevertheless, bats can achieve robust navigation with a small brain in complex environments, i.e. avoiding randomly located obstacles and flying with other conspecifics [1–4]. Here, the term “cheap design” refers to a concept, based on studies of mobile robots, that entails low calculation cost and simple mechanical design [5, 6]. If the decision-making process of echolocating bats that is used for 3D path planning in real time from low-dimensional acoustic sensor inputs can be modelled with simple mechanical design, it is expected to lead us to create a bat-inspired navigation system supporting cheap design mobile robots.

In order to negotiate a complicated environment using a restricted acoustic field of view with a simple mechanical design, bats may employ not only physiological specialization of their auditory systems [7, 8] but also behavioral strategies [9] of temporal-spatial scanning adapted for the capacity of the scanning range. The dynamics of the relationship between “acoustic gaze” (direction of ultrasound pulses emitted by bats) and bats’ flight control has been investigated by using aerial-feeding echolocating bats [10–14]. However, it remains unclear how bats can be operated the temporal-spatial scanning in an intuitive and efficient way. Our motivation is to understand the behavioral usefulness of the bats for the temporal-spatial scanning throughout the development of the autonomous vehicle which can be evaluate in conjunction with practical acoustical sensing problems in real environments.

In this study, we embedded the algorithm inspired by bats in an autonomous vehicle equipped with simple ultrasonic sensors (one transmitter and two receivers). Then, vehicle performance was experimentally investigated in obstacle environment. Finally, the numerical simulation was conducted to quantify that the algorithm inspired by bats was robust to the practical sensing problems.

2 Vehicle Experiment

2.1 Purpose

In a previous study, during the flight in unfamiliar space, we have often observed the double- and triple pulse (a set of two and three pulses emitted with short interval) scanning of bats, the direction of pulse emission of which was alternately shifted between the intended flight direction and the nearby obstacle’s direction. Such an alternate shifting of the pulse direction has been confirmed in many bats that fly in various obstacle environments, as shown in Fig. 1. To investigate how selective spatial scanning with multiple pulses contributed to improving the robustness of navigation based on cheap design sensing, a double-pulse scanning method was proposed as a bat-inspired navigation algorithm. In the double-pulse scanning method, (1) the direction of pulse emission was alternately shifted between the direction of movement and the direction of the nearest obstacle, and (2) the direction of movement was calculated for every double-pulse emission based on integrated information from all echoes detected by double-pulse sensing. To quantify the double-pulse scanning method, a conventional scanning method

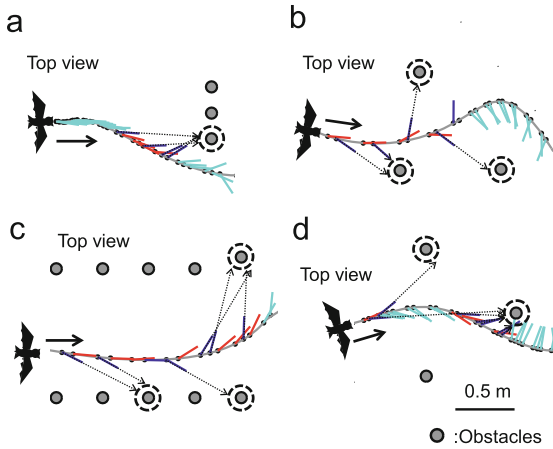


Fig. 1. Examples of pulse direction control by four different individual bats during flight in various obstacle environments. Measurement procedure was described in our previous paper [15]. Each bat was observed only one time (<20 s), focusing on exploratory behavior in an unfamiliar place. Red and blue lines indicate that the pulses were alternately emitted towards the bats' own flight direction (red) and the obstacle direction (blue). Light blue lines indicate any other pulses that the bats' intention could not be estimated. Because the emission pulse was a broad beam, we considered bats to have aimed the pulse emissions towards the target obstacles as long as the pulses were directed towards the dashed-line circles the diameters of which are 16 cm. As a result, all of these aiming pulses were emitted towards the target with an angle deviation within 7 degrees. (Color figure online)

was also developed, in which: (1) the pulse direction was fixed in the direction of travel of the car body and (2) the moving direction was calculated for every pulse emission.

2.2 Vehicle Design

We made a mobile vehicle (30 (H) × 15 (W) × 25 (L) cm), which consisted of three ultrasonic sensor units, one transmitter (MA40S4R; Murata, Kyoto, Japan, $\pm 50^\circ$ at 6 dB off-axis angles from the centre of the beam direction), two receivers (SPM0404UD5; Knowles, Itasca, IL, USA), two servomotor units, and a central processing unit (Arduino LLC, Somerville, MA, USA; $f_s = 140$ kHz). One of the servomotors controlled the pulse direction from the transmitter and the other servomotor was connected to the right and left front wheels shaft so that the pulse direction could be adjusted independently of the control of the vehicle driving direction.

Our used piezoelectric sensor was difficult to emit a wideband FM signal similar to the bats; hence, the transmitter emitted a short duration tone burst signal that had a frequency of 40 kHz and 2 ms duration. The sound pressure level of the pulse was 103 dB at a distance of 1 m in front of the transmitter. The vehicle was designed to extract echo arrival timings for all echoes detected per emission, ranging from 2 to 30 ms from pulse emission, corresponding to detection distances of 34 cm to 5.1 m (note that the minimum value was set at 2 ms to avoid temporal overlap of emitted pulse and echo). While

driving, the echo arrival timings at the right and left receivers (t_{right}, t_{left}) were determined by reading the instant timing when the amplitude value of the echo exceeded the voltage threshold. It should be noted that, when the echoes returning from different objects were temporally overlapped, only the fastest arrival timing was regarded as the echo arrival time, and the arrival times of the subsequent overlapping echoes were ignored. The position of each obstacle was localized using Eqs. (1) and (2) in real time, respectively.

$$r_{obs}(t, n) = \frac{c(t_{right}(t, n) + t_{left}(t, n))}{4} \quad (1)$$

$$\theta_{obs}(t, n) = \arcsin \frac{c(t_{right}(t, n) - t_{left}(t, n))}{d} + \varphi_p \quad (2)$$

where d indicates the distance between the right and left receivers which was set on 8 cm, t indicates the pulse emission timing, n indicates the order in which echoes are detected by each receiver, r_{obs} is the distance from the vehicle to the obstacle, φ_p is the direction of the emission pulse relative to the vehicle driving direction, and θ_{obs} is the direction of the obstacle relative to the vehicle driving direction. Because the echoes arriving at the right and left receivers were paired in time-sequence order to calculate r_{obs} and θ_{obs} using Eqs. (1) and (2), they were sequentially numbered; thus, the n of r_{obs} and θ_{obs} were defined as $r(t, n)$ and $\theta(t, n)$, respectively. Here, the number of all obstacles detected by the pulse emission at time t is defined as $N(t)$ for calculation of the vehicle navigation algorithm.

The vehicle was controlled based on two simple movements: (1) moving straight forward and (2) pivoting in place (without moving forward) to change the driving direction. Figure 2a and b provide schematic diagrams of the control dynamics for moving direction φ_d with the conventional scanning method and double-pulse scanning method, respectively. The timing of the i^{th} pulse emission is defined as t_i . The moving direction φ_d of the conventional scanning method was changed by pivoting after pulse emission, with a response time Δt including both mechanical and echo processing time (Fig. 2a). On the other hand, the moving direction φ_d in the double-pulse scanning method was calculated for every double-pulse emission (Fig. 2b). Then, the vehicle moved straight forward for a duration τ , which was set at 0.6 s in the conventional scanning method and 1.2 s in the double-pulse scanning method. Because the response time Δt (< 0.1 s) was sufficiently shorter than τ , we could consider the inter-pulse interval to be 0.6 s for both the conventional and double-pulse scanning methods, with the result that the inter-pivot interval (inter-pivot distance) of the double-pulse scanning method was twice as long as that of the conventional scanning method. The vehicle driving speed was set at ~ 15 times slower (21 cm/s) than flight speed of *R. ferrumequinum nippon* during obstacle-avoidance flight. Therefore, the inter-pulse interval of the vehicle was set at 0.6 s, which was approximately 15 times that of the bats' inter-pulse interval.

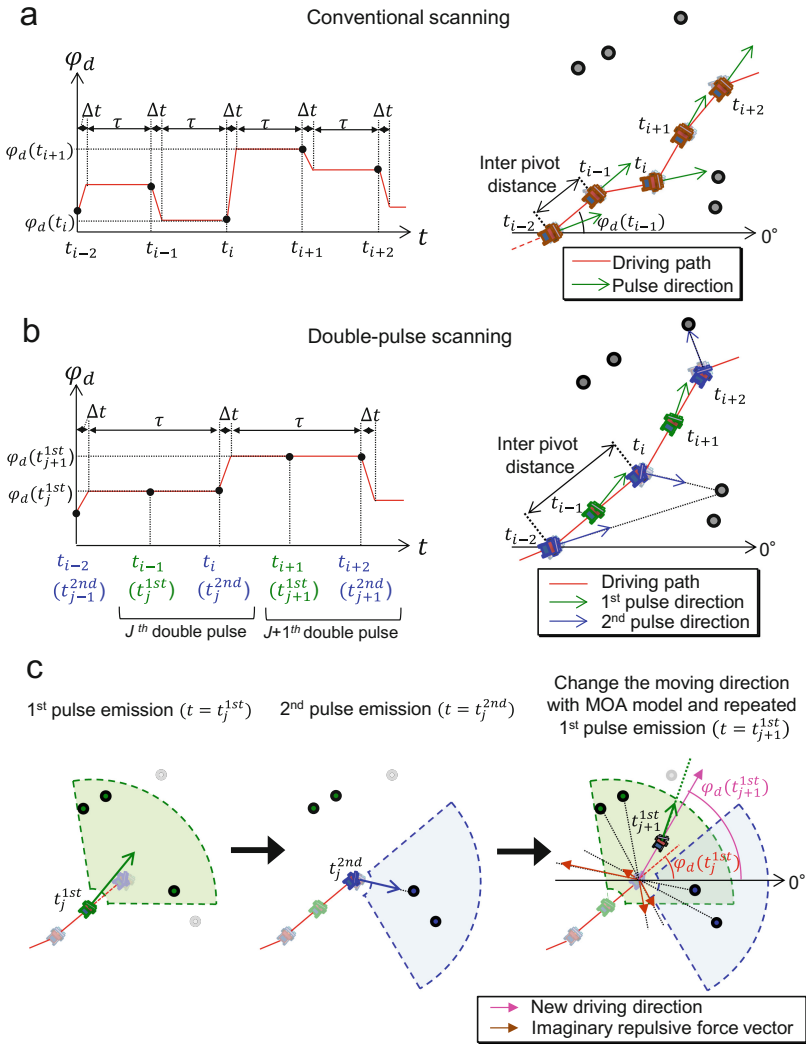


Fig. 2. Comparison of vehicle movement between the conventional scanning system and the double-pulse scanning system. Schematic of temporal change in moving direction φ_d of the vehicle with the conventional scanning (a) and double-pulse scanning (b). The conventional scanning system repeated the pivot turn in the duration of response time Δt toward the calculated moving direction at every sensing. In contrast, the double-pulse scanning system was set for pivot turns every double-pulse emission. (c) Schematic of control law for pulse direction φ_p in the double-pulse scanning system. The 2nd pulse emission was directed towards the nearest obstacle among all obstacles detected by the previous two successive emissions, i.e. the 1st pulse emission of the j^{th} double pulse and the 2nd pulse emission of the $(j - 1)^{\text{th}}$ double pulse. Then, the direction of the 1st pulse emission of the $(j + 1)^{\text{th}}$ double pulse, $\varphi_p(t_{j+1}^{1st})$, was determined based on the amount of change in the moving direction φ_d between j^{th} and $(j + 1)^{\text{th}}$ double pulses.

2.3 Vehicle Navigation Algorithm

First, we constructed an obstacle-avoidance model for both the conventional and double-pulse scanning methods to control the vehicle’s moving direction using multiple obstacle information (multi-obstacle-avoidance [MOA] model. See Appendix). To explain the MOA model briefly, we determined the moving direction φ_d in the case of the conventional scanning method using the following equation (Fig. 2a):

$$\varphi_d(t_{i+1}) = \arg(e^{i\varphi_d(t_i)} - 2 \sum_{n=1}^{N(t_i)} \sqrt{\frac{\alpha}{r(t_i, n)}} \sin\left(\arctan\frac{r(t_i, n)}{k}\right) e^{i\theta(t_i, n)}) \quad (3)$$

where $k = 1.3$ m, $\alpha = 0.015625$ m and \arg means a function operating on complex numbers (symbol i in the exponents means imaginary unit) which gives the angle from real axis ($=0^\circ$). The moving direction φ_d was changed after the i^{th} pulse emission. On the other hand, in the case of double-pulse scanning method, after the 2nd pulse emission of the j^{th} double pulse, φ_d could be determined using the following equation (Fig. 2b):

$$\begin{aligned} \varphi_d(t_{j+1}^{1st}) &= \arg(e^{i\varphi_d(t_j^{1st})} - 2 \sum_{n=1}^{N(t_j^{1st})} \sqrt{\frac{\alpha}{r(t_j^{1st}, n)}} \sin\left(\arctan\frac{k}{r(t_j^{1st}, n)}\right) e^{i\theta(t_j^{1st}, n)}) \\ &- 2 \sum_{n=1}^{N(t_j^{2nd})} \sqrt{\frac{\alpha}{r(t_j^{2nd}, n)}} \sin\left(\arctan\frac{k}{r(t_j^{2nd}, n)}\right) e^{i\theta(t_j^{2nd}, n)}. \end{aligned} \quad (4)$$

where $k = 1.3$ m and $\alpha = 0.0078125$ m. Thus, the moving direction φ_d in the double-pulse scanning method was calculated using all obstacle information obtained from the 1st and the 2nd pulse emissions. It should be noted that the positions of obstacles detected by the 1st pulse emission were corrected according to the movement of the vehicle to calculate the φ_d . In the double pulse scanning method, the parameter k was set to be the same value as that of the conventional scanning method. However, the parameter α was set to half the value of the conventional scanning method, since the proposed method was subjected to a more repulsive force by double sensing. It was confirmed that the vehicle operate the almost same avoidance path in those proposed method and the conventional scanning method when the obstacle pole placed at 1 m in front of the vehicle.

In the MOA model of both the conventional and double-pulse scanning methods, the moving direction φ_d can be calculated by adding the imaginary attraction force vector of the vehicle’s current driving direction and imaginary repulsive force vectors. The imaginary repulsive force produced from each obstacle was determined by the distance $r(t, n)$ and the direction $\theta(t, n)$ ($n = 1, \dots, N(t)$) of the obstacles. Furthermore, by assuming the imaginary width of individual obstacles according to the distance $r(t, n)$, the MOA model calculates the imaginary repulsive force, which is inspired to the concept of monoscopic depth cues of the visual sensing (i.e. the perceived object size

changes with distance). As a result, the driving direction can be defined by adding reconstructed imaginary two-dimensional images of surrounding objects that were derived from one-dimensional sound information.

In the conventional scanning method, the pulse direction was fixed in the direction of travel of the car body at all times for every pulse emission (Fig. 2a). In the double-pulse scanning method, the direction of the 1st pulse emission of the $(j + 1)$ th double pulse, $\varphi_p(t_{j+1}^{1st})$, was determined by the amount of change in the moving direction between the j th and $(j + 1)$ th double pulses (Fig. 2c).

$$\varphi_p(t_{j+1}^{1st}) = \varphi_d(t_{j+1}^{1st}) + \beta \left(\varphi_d(t_{j+1}^{1st}) - \varphi_d(t_j^{1st}) \right), \quad (5)$$

where β was set at 0.6. After the vehicle detected the obstacles by the 1st pulse emission, the 2nd pulse emission was directed to the nearest obstacle among all obstacles detected by the previous two successive emissions, i.e. the 1st pulse emission of the $(j + 1)$ th double pulse and the 2nd pulse emission of the j th double pulse. As a result, in the double-pulse scanning method, the direction of pulse emission alternates between the direction of movement and the direction of the nearest obstacle, simulating the movement of bats flying in unfamiliar spaces. Figures 3a and b show flowcharts of the avoidance algorithm based on the MOA model for the conventional scanning and double-pulse scanning methods, respectively. The frequency of decision making for movement direction in the double-pulse scanning method was half that in the conventional scanning method. On the other hand, avoidance direction could be calculated using twice as much obstacle information by spatial integration obtained from double-sensing.

2.4 Experimental Method

An obstacle course was constructed by arranging plastic poles (12 cm diameter) in a 4×2 m driving field. While driving on the obstacle course, obstacle distance and direction localized by the vehicle, and the pulse direction of the transmitted signal, were stored instantly in memory on the vehicle, and then transmitted using wireless serial communication (X-bee; Digi International Inc., Minnetonka, MN, USA) to a personal computer in real-time. In addition, the vehicle driving path and moving direction were measured externally using two digital high-speed video cameras, with the same recording procedure used in the behavioural experiments with bats. The vehicle has a LED light that flashed in synchronization with pulse emission, so that the actual pulse emission timing could also be recorded by these video cameras. The localization errors of $r(t, n)$ and $\theta(t, n)$ ($n = 1, \dots, N(t)$) were evaluated using the differences between the localized values from the vehicle and the values measured by the external cameras at every pulse emission. Furthermore, the obstacle-avoidance performance of a vehicle was measured to permit comparison between the conventional scanning and double-pulse scanning methods.

For statistical comparisons, a Mann–Whitney U -test and a Student's t -test were used, where appropriate, to test for significant differences in obstacle localization accuracy, the number of detected obstacles, N , and detection rate of the nearest obstacle from the

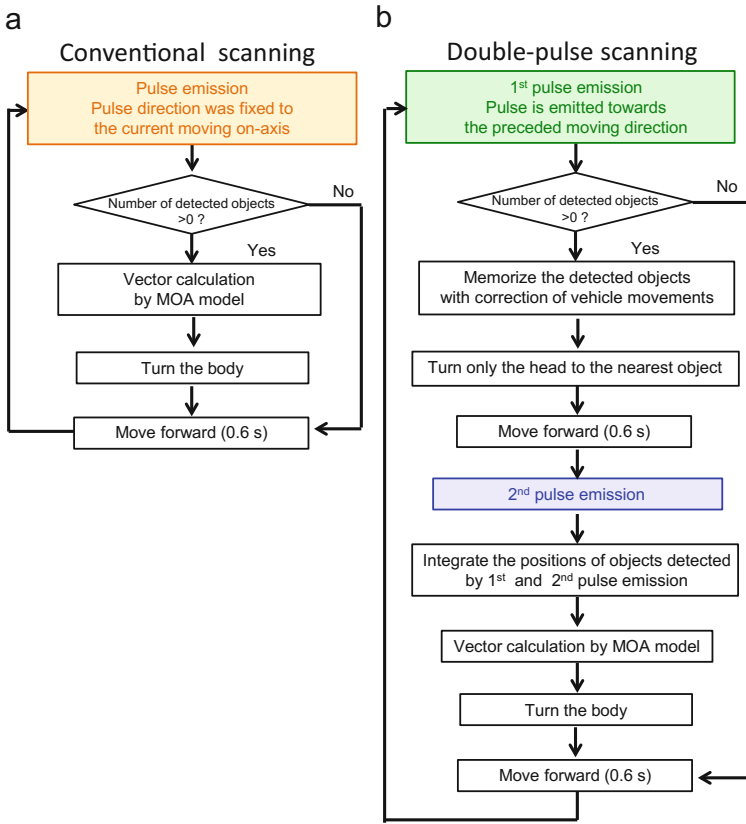


Fig. 3. Schematic diagrams of vehicle navigation algorithms. (a) Conventional scanning system. (b) Double-pulse scanning system.

vehicle position between the double-pulse scanning method and the conventional scanning method.

2.5 Result of the Vehicle Experiments

Examples of the moving path and pulse direction of the vehicle while driving on the obstacle course are shown in Figs. 4a and b, respectively. With the conventional scanning method, the vehicle collided with the pole located at the centre of the obstacle course even though the vehicle detected the pole (Fig. 4a), whereas the double-pulse scanning method could avoid the pole (Fig. 4b). Figures 10c and d also show vehicle driving paths taken from the first 10 trials in each method. Vehicle collision frequently occurred at the centre pole with the conventional scanning method, but centre pole was avoided with the double-pulse scanning method in all of 10 trials. The total success rates for the 100 obstacle-avoidance trials (i.e. the proportion of trials where the vehicle successfully avoided collisions) on this course were 13% (13/100 trials) for the

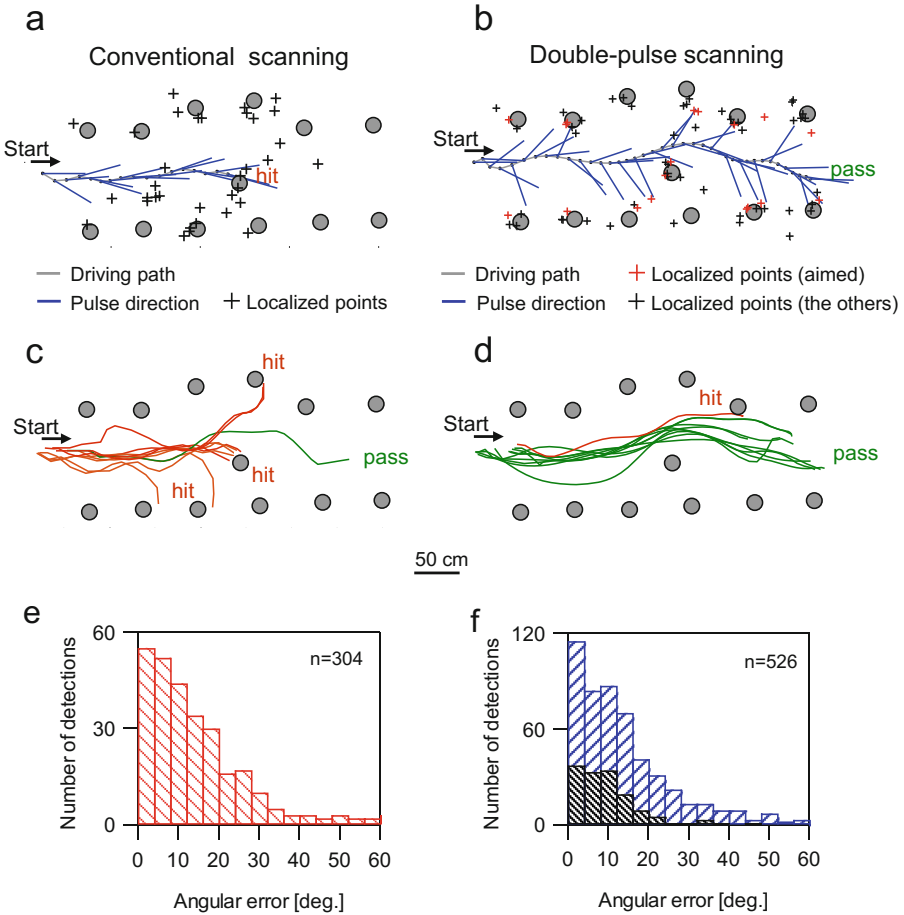


Fig. 4. Demonstration of vehicle navigation during obstacle-avoidance driving. Top views of representative driving trajectories (red line) and pulse directions (blue line) for the conventional scanning system (a) and the double-pulse scanning system (b). All obstacle positions localized by the vehicle are shown with cross-marks. Red cross-marks in the results of the double pulse scanning system indicate the nearest obstacle positions localized by obstacle-aimed pulse emission. (d, c) Top views of driving trajectories for the conventional scanning system (c) and double-pulse scanning system (d) (10 trials per system). (e, f) Distributions of error angle for obstacle detection in the conventional (e) and double-pulse scanning systems (f). It should be noted that the error angle of the nearest obstacles localized by the obstacle aiming pulse in the double-pulse scanning system was also indicated by a black histogram. (Color figure online)

conventional method and 73% (73/100 trials) for the double-pulse scanning method. The collisions in each method were categorized into two types: collisions with the centre obstacle pole (52% for conventional and 10% for double-pulse) and collisions with the right- and left-side poles (35% for conventional and 17% for double-pulse).

In Fig. 4a and b, the positions of all obstacles localized by the vehicle are marked with crosses. The localized positions, however, deviated from the actual obstacle positions; the localization error for the first 10 trials was 19 ± 12 cm in the conventional scanning method and 20 ± 12 cm in double-pulse scanning method, a non-significant difference (Mann–Whitney U -test, $P = 0.07$). Furthermore, Fig. 4e and f show the distributions of the angular error of detected obstacles for the 10 trials in Fig. 4c and d. The angular error of the conventional method was not significantly different from that of the double-pulse scanning method (Mann–Whitney U -test, $P = 0.54$). However, in the double-pulse scanning method, the localized position focused by the 2nd pulse emissions of the double pulse directed toward the nearest obstacle (see red cross-marks in Fig. 10b) had a significantly lower angular error (see black histogram in Fig. 4f, Mann–Whitney U -test, $P < 0.01$) and distance error (Mann–Whitney U -test, $P < 0.01$) compared with the other localized positions and this was also significantly lower than that of the conventional method (Mann–Whitney U -test, $P < 0.01$). These results suggest that obstacle-aimed pulse emission improves the localization accuracy for the target obstacle.

The distributions of the number of obstacles N used to calculate moving direction are shown in Fig. 5a. The mean N was 4.5 ± 1.3 in double-pulse scanning, which was almost twice that in conventional scanning ($N = 2.0 \pm 1.0$) owing to the integration of obstacle information obtained from double sensing (Mann–Whitney U -test, $P < 0.01$). In the double-pulse scanning method, the angles θ_{obs} of detected obstacles relative to pulse direction were distributed mainly around the centre of the pulse's own acoustic field (Fig. 5c), whereas the conventional scanning method tended to detect obstacles to its own right or left off-axis sightline (Fig. 5b). Moreover, the detection rate of the nearest obstacle from the vehicle position reached $\sim 80\%$ (334/526) in the double-pulse scanning method, which was significantly higher than that in the conventional scanning method (50%, 186/304, Student's t -test, $P < 0.05$) (Fig. 5d).

These findings suggest that the double-pulse scanning method has several practical advantages for obstacles detection, for example, allowing vehicles to drive without losing the nearest obstacle within the acoustic field of view, even when the frequency of decision making with respect to movement direction was reduced by half.

3 Numerical Simulation

3.1 Simulation Situation

In the previous chapter, we experimentally revealed that vehicles with proposed methods improve the robustness of the path planning comparing to those without proposed methods. Although, vehicle experiment has not been revealed certain factors that improve the robustness of path planning. In order to clarify this, the numerical simulation was conducted in the same situation as the vehicle experiment. In particular, obstacle course arrangement, moving speed of simulated vehicle (21 cm/s) and inter-pulse interval (0.6 s) were set in the same way as the vehicle experiment situation.

Furthermore, the obstacle detection range was also estimated to be similar to the practical sensing situation by using the actually measured pulse and receiver directivity

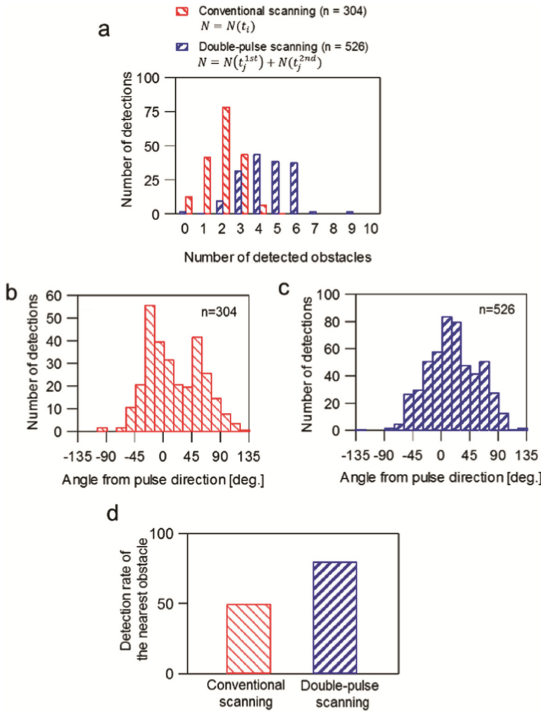


Fig. 5. Comparison of obstacle-detection performance between the conventional and double-pulse scanning systems for the first 10 trials. (a) Distributions of the number of obstacles N that were used to calculate moving direction in the conventional and double-pulse scanning systems. Distributions of obstacle-detection angle from the pulse direction in the conventional (b) and double-pulse scanning system (c). (d) Comparison of detection rates of the nearest obstacles, according to vehicle coordination, between the conventional and double-pulse scanning systems.

pattern (Fig. 6a and b) and the distance attenuation characteristics of the pulse (Fig. 6c). Those pulse directivity patterns and the distance attenuation characteristics of the pulse were fitted by Gaussian and exponential functions as following equations

$$F(r_{obs}(t, n)) = k_{f1} + k_{f2} \cdot e^{k_{f3} \cdot r_{obs}(t, n)} + k_{f4} \cdot e^{k_{f5} \cdot r_{obs}(t, n)}, \quad (6)$$

$$G(\theta_{obs}(t, n)) = 1 / \left(k_{g1} + k_{g2} \cdot e^{\left(\frac{\theta_{obs}(t, n)}{k_{g3}} \right)^2} \right), \quad (7)$$

where $k_{f1} = 0.012658829$, $k_{f2} = 0.261003066$, $k_{f3} = -3.065341475$, $k_{f4} = 2.441670304$, $k_{f5} = -23.2536802$, $k_{g1} = 0.00658$, $k_{g2} = 1.009079$ and $k_{g3} = 59.94135$. By using Eqs. (6) and (7), from the distance $r_{obs}(t, n)$ and the direction

$\theta_{obs}(t, n)$ of the obstacle, echo strength level $P_e(t, n)$ in each obstacle was estimated by assuming it as total internal reflection with following equation

$$P_e(t, n) = 20\log_{10}(2F(r_{obs}(t, n)) \cdot G(\theta_{obs}(t, n))) \tag{8}$$

where echo strength level $P_e(t, n)$ is respect to the strength of the pulse. When the calculated echo strength level $P_e(t, n)$ was higher than minimum strength level for echo detection (P_{min}), the obstacle was regarded as detected. It should be note that minimum strength level for echo detection P_{min} was determined as -36 dB from the maximum detection range of the actual vehicle in this study. As a result of these estimations, obstacle detection range was reproduced, shown in Fig. 6d, without setting an unreasonable detection range such as a fan shape.

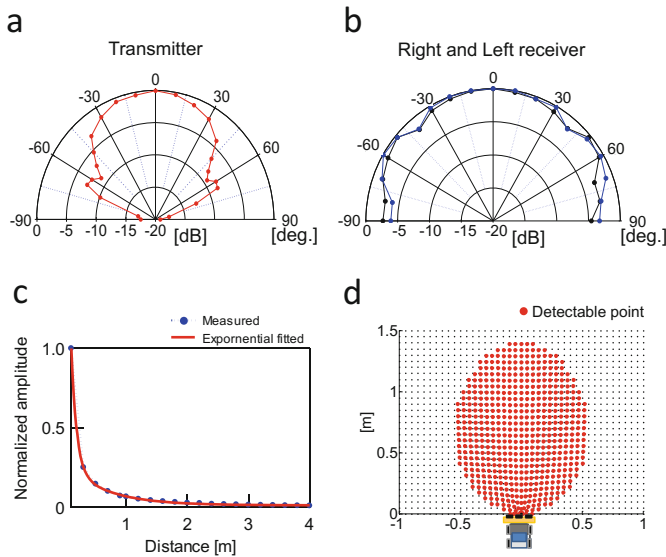


Fig. 6. Detection range estimation based on the actual sensors characteristics. (a, b) Directivity pattern of the transmitter (red line), right (blue line) and left receivers (black line) which were measured by using 40 kHz constant frequency sound. (c) Distance attenuation characteristic of the propagation sound of 40 kHz. The actual measured distance attenuation pattern (blue line-plots) was fitted by exponential curve-fitting (red line). (d) Estimated detectable range (red plots) for the vehicle simulation by using the gauss-fitted directivity pattern of the transmitter and the curve-fitted distance attenuation characteristic. (Color figure online)

3.2 Simulation Method for Ideal and Practical Condition

To quantify the robustness for the sensing ambiguity, the numerical simulation was conducted in different two conditions. The one was the ideal sensing condition which can be localized the detection point to the accurate obstacle position. The other one was the practical sensing condition which included the localization ambiguity (1) due to the

interference problem of echoes returned from multiple objects and (2) due to sensing performance of the vehicle.

Echoes interference problem was implemented based on practical sensing problem, in which the subsequent echo was made blinded when that arrives within the duration (2 ms) of the preceding echo. As a fatal problem related to this, echo-pairing mismatching was also implemented when the order of the echo sequence was different between the right and left receivers (Fig. 7a and b). In this paper, Localization error due to the mismatched echo-pairing was defined as ghost localization.

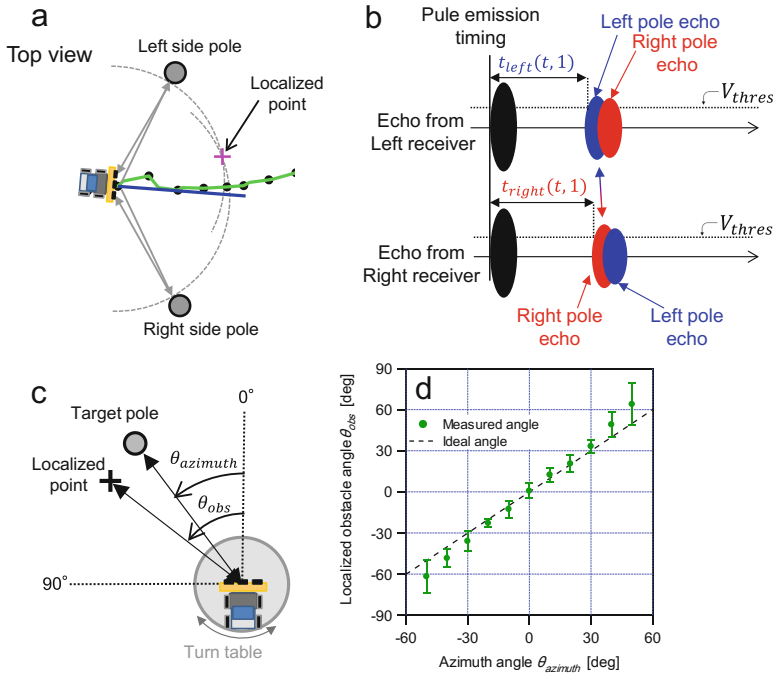


Fig. 7. Actual sensing problems including the ghost localization and sensing resolution reflected in the simulation of the practical condition. (a) Actual case of the ghost localization caused by miss-pairing the multiple echoes reflected from right and left-side poles. (b) Schematic diagram of echo sequence order of the right and left receivers in the situation of (a). Echoes from right receiver were arrived in the order of right side pole and left side pole, whereas the left receiver shows that echoes' order were inversely. (c) Measurement procedure for the directional error of the localized obstacle angle θ_{obs} depending on the azimuth angle of the obstacle $\theta_{azimuth}$ in stationary condition. (d) Average localized angle depending on actual azimuth angle by 100 repeated sensing in each condition. Error bar indicates the standard deviation for 100 localization and dashed line indicates the ideal localized angle for each azimuth angle. (Color figure online)

For embedding the localization ambiguity due to the sensing resolution of the vehicle into the numerical simulation, a characteristic of directional error of localization with respect to the obstacle azimuth angle was measured in stationary condition by using the vehicle (Fig. 7c). As you can see in Fig. 7d, the direction error of localization was

increased by increasing the obstacle azimuth angle. By fitting the characteristics of the average and distribution of the direction error to the Lorenz curve, localization ambiguity was embedded into the numerical simulation as following equation

$$\theta_{obs}(t, n) \sim N\left(\mu(\theta_{azimuth}(t, n)), \sigma(\theta_{azimuth}(t, n))^2\right), \tag{9}$$

$$\mu(\theta_{azimuth}(t, n)) = \theta_{azimuth}(t, n) \left(1 + \frac{k_{\mu1} + k_{\mu2} e^{-\frac{\theta_{azimuth}(t, n) - k_{\mu3}}{k_{\mu4}}}}{|\theta_{azimuth}(t, n)|} \right), \tag{10}$$

$$\sigma(\theta_{azimuth}(t, n)) = k_{\sigma1} + k_{\sigma2} e^{-\frac{\theta_{azimuth}(t, n) - k_{\sigma3}}{k_{\sigma4}}}, \tag{11}$$

where $k_{\mu1} = 156.1898301044632$, $k_{\mu2} = -155.3931174799931$, $k_{\mu3} = -0.2661352979727751$, $k_{\mu4} = 177.4961370454644$, $k_{\sigma1} = 183.209814430525$, $k_{\sigma2} = -179.1180618723616$, $k_{\sigma3} = -3.635825346353006$, $k_{\sigma4} = 234.4054352819113$.

By comparing the specific performance in proposed and conventional methods between the ideal condition and practical sensing condition, influence of the sensing ambiguity was investigated.

3.3 Results of Numerical Simulations

Figure 8a and b shows representative moving path, pulse direction and localized points simulated in ideal sensing condition by using conventional and proposed methods, respectively. As a result of 200 times simulation by changing the initial start position, the total success driving rates were 50% for the conventional method and 58% for the double-pulse scanning method (Fig. 8c). Therefore, the ideal simulation could not reproduce the success rate differences shown in vehicle experiment (13% for conventional and 73% for double-pulse).

On the other hand, for the practical sensing conditions, the localized points tend to be distributed in both scanning methods, which was similar to the vehicle experiments (Fig. 8d and e). As a result of 200 repeated trials at each 8 start position where both scanning methods were successfully operated under ideal conditions, the success rate was 36% for the conventional method whereas 55% for the double-pulse scanning method (Fig. 8f), suggesting that the success driving rate of the conventional method was lower than that of the proposed method, as shown in the vehicle experiment.

Figure 9a shows occurrence probability of ghost localization for every pulse emissions in each scanning method. The mean ghost localization probability was $2 \pm 2\%$ in double-pulse scanning whereas $8 \pm 4\%$ in conventional scanning. Therefore, the double-pulse scanning method suppressed the ghost localization occurrence comparing to the conventional scanning method (Mann–Whitney *U*-test, $P < 0.01$). Furthermore, an

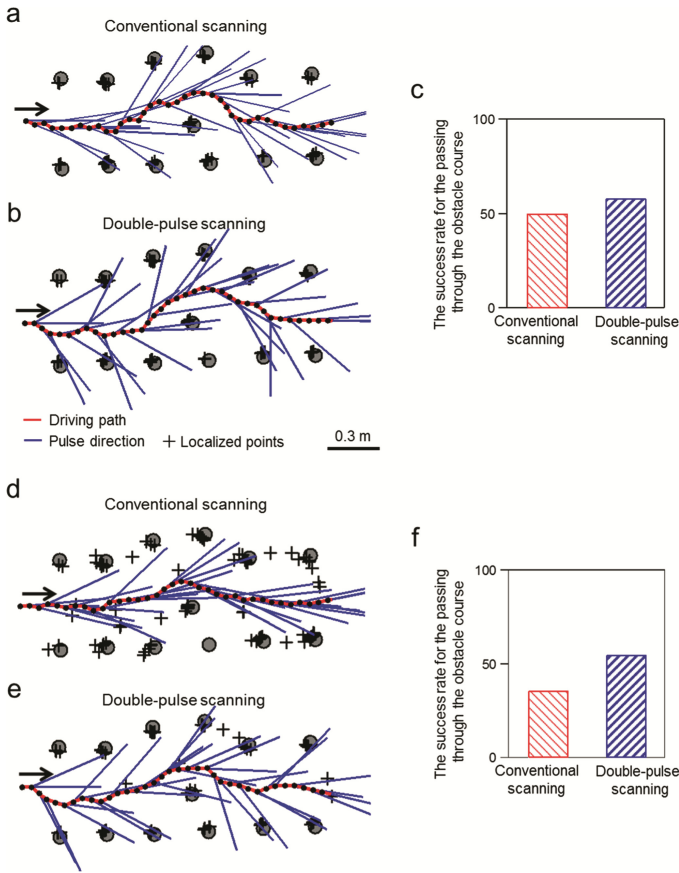


Fig. 8. Simulation of the vehicle navigation during obstacle-avoidance driving in the case of ideal condition and practical condition. Top views of representative driving trajectories (red line), pulse directions (blue line) in the case of ideal condition for the conventional scanning method (a) and the double-pulse scanning method (b). Note that all obstacle positions localized by the vehicle are shown with cross-marks. (c) A comparison of the success rate for the passing through the obstacle course between the conventional and double-pulse scanning methods. In this analysis, 200 times simulations were conducted for each scanning methods by changing the initial start position. Then, extracted 8 starting positions where both scanning methods were successfully operated under ideal conditions, the same analyses were also conducted by the practical condition, which results were shown in (d, e, f). (Color figure online)

avoidance direction calculated from accurate obstacle coordinates is defined as an ideal avoidance direction, the directional error of the avoidance direction was also evaluated for each scanning method as shown in Fig. 9b. As a result, the directional error of the avoidance direction was $6 \pm 7^\circ$ in the double pulse scanning method whereas $9 \pm 11^\circ$ in conventional method, indicating that the directional error of the double pulse scanning method is smaller than that of conventional methods (Mann–Whitney *U*-test, $P < 0.01$).

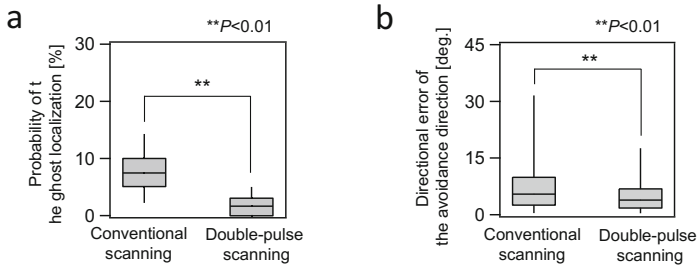


Fig. 9. Comparison of obstacle-detection performance between the conventional and double-pulse scanning methods in the case of practical condition. (a) Occurrence probability of the ghost localization for the every sensing in the conventional and double-pulse scanning methods. (b) Angular error for the avoidance direction in the conventional and double-pulse scanning methods.

These findings suggest that the double-pulse scanning method is a robust navigation method against external disturbances included in actual acoustic sensing such as the localization ambiguity and the ghost localization due to overlapping echoes.

4 Discussion

In the present study, with reference to our observed behavioral pattern of bats which shifts the direction of the double-pulses between nearby obstacle and moving directions during the obstacle avoidance flight, we constructed a bat-inspired algorithm double-pulse scanning method. As a result, we demonstrated that the behavioral ingenuity exhibited by bats during echolocation also helped minimal designed vehicles to avoid obstacles.

In fact, we found that the double-pulse scanning method improved the avoidance performance of the autonomous vehicle by conducting the practical experiment. In the conventional scanning method, in which the pulse direction was always fixed to the current driving on-axis, the immediate obstacle was often outside of the angle of the detection range when the vehicle changed direction to avoid a previous obstacle. As a result, the detection rate of immediate obstacles was approximately 50% (Fig. 5d). In contrast, the double-pulse scanning method, mimicking the bats' behavior, could eliminate such a "blind spot" by keeping the critical obstacle point within the acoustic field of view, which was spatially expanded by double-pulse sensing. This is one of the effects of the integration of spatial information provided by the double-pulse sensing method. Furthermore, the vehicle calculates its own moving direction using not only immediate obstacle information, but also more distant obstacle information: this allows the vehicle to select a more robust avoidance path (Fig. 4d).

Moreover, the double-pulse scanning method allows the vehicle to double-count a specific obstacle using two emissions. Since the imaginary repulsive force is calculated using all of the detected obstacles, the double-pulse scanning method gives weights to obstacles that are detected twice to guide the driving direction. This is considered

temporal integration of obstacle information, which is another advantage of the double-pulse scanning method, as double-counted obstacles were usually located near the driving path. As a result, the double-pulse scanning method extends not only spatially but also temporally its own vehicular acoustic field of view.

In a previous study, *Eptesicus fuscus* was found to produce sonar sound groups (i.e., double pulses) more often in complex environments or when performing complicated tasks [16–18]. The emission of sonar sound groups has been reported in a number of bat species, which suggests that exercising temporal control over emissions helps bats negotiate complex or unfamiliar environments [19]. In particular, it was suggested that the emission of double pulses allows bats to obtain immediate and more detailed surrounding information for planning flight paths [17] or for improving the resolution of an uncertain target's position [16]. Our vehicle demonstration and numerical simulation also supported the idea that multiple pulse emissions with information integration are efficient for complex environment navigation. From the viewpoint of an actual localization problem, large errors of localization have often occurred owing not only to the capability of the sensing resolution, but also to unintended correct combination problems of echo paring which was named ghost localization (Fig. 7a). Our numerical simulations represent that the proposed method suppresses the interference of echoes returning from multiple objects by selecting the pulse direction toward to the targeting obstacle (Fig. 9a). Even in the previous simulation research of the three dimensional localization mechanism of bats, similar results have been reported that adjustment of direction of attention with ear movements is efficient to accurately localize the obstacles positions [20]. Moreover, in our proposed method, even if the interference occurred in one of the double sensing processes, the influence of the localization error due to a mismatch of echo combinations can be reduced by integrating the twice-sensed information that was obtained by scanning at a slightly moved position. As a result of such a localization error reduction, the directional error of the avoidance direction was also suppressed (Fig. 9b). These numerical simulations indicate that the proposed method can be robust path planning against to the localization ambiguity. Though the double-pulse scanning method reduces the frequency of the decision making regarding the direction of movement to half that of the conventional scanning method (Fig. 2), our findings suggest that the integration of information from two emissions is effective; i.e. acoustic detection restricted to only one transmitter and two receivers, demonstrating that the ingenuity inspired by bats has a large effect on simple design sensing.

The recent trend in spatial sensing technology is to increase the number of sensor units so that the whole of the surrounding space can be covered by integrating the spatial information of multiple sensors. On the other hand, the vehicle in the present study has only one transmitter and two receivers. In this study, we demonstrated a method to collect and integrate spatial information regarding the external world inspired by the observation of the echolocating bats. Because the proposed double-pulse sensing uses simple algorithms based on temporally and spatially integrated obstacle information, it can be applied readily to various navigation methods with modest calculation costs. For example, simulation research for the humanoid robot navigation with stereo vision has demonstrated that control of alternate gaze shifting between the direction of movement and the direction of an obstacle is effective to avoid collision against critical obstacles

[21]. Even in the animal research, behavior regarding spatial perception has been studied extensively in visually guided animals through measurements of eye movement (humans) or head angle (flies, birds) [22–24]. With reference to those researches, we can compare gaze control by vision-guided animals with simple acoustic sensing inspired by the bat bio-sonar method. The basis of our idea may provide new insight into not only method for representative ultrasonic sensing relying on cheap and simple methods but also other sensing technologies for spatial perception. We suggest that the processes of decision making and conception observed in higher animals offer new insight into future biomimetic research.

Acknowledgements. This work was supported by JSPS KAKENHI Grant Numbers JP16H06542 (Grant-in-Aid for Scientific Research on Innovative Areas) to SH, and JP17H07242 (Grant-in-Aid for Research Activity Start-up) to YY, and by the Japan Science and Technology Agency PRESTO program to SH.

Appendix: MOA Model

In this appendix, we briefly show our method for determining the direction of movement after echolocation. The basic idea of the MOA model in the case of the conventional scanning method is shown schematically in Fig. 10. After the i^{th} pulse emission at time t_i , the vehicle changes its moving direction, and the new moving direction is determined according to the weighted sum of the vector of the current driving direction and imaginary repulsive force vectors arising from the recognized obstacles. We set the repulsive force from obstacle n , described as the integration of the imaginary pressure $g(r(t_i, n))$ with respect to viewing angle θ from $\theta(t_i, n) - W(r(t_i, n))$ to $\theta(t_i, n) + W(r(t_i, n))$. Thus, the new moving direction $\varphi_d(t_{i+1})$ is described by the following equation:

$$\varphi_d(t_{i+1}) = \arg \left(e^{i\varphi_d(t_i)} - \sum_{n=1}^{N(t_i)} \int_{\theta(t_i, n) - W(r(t_i, n))}^{\theta(t_i, n) + W(r(t_i, n))} g(r(t_i, n)) e^{i\theta} d\theta \right), \quad (12)$$

where $N(t_i)$ indicates the number of recognized objects at $t = t_i$. It should be noted that the positions of the recognized objects are calculated with the echolocation method. The distance factor $g(r(t_i, n))$ and the obstacle window factor $W(r(t_i, n))$ are given by following equations, respectively:

$$g(r(t_i, n)) = \sqrt{\frac{\alpha}{r(t_i, n)}} \quad (13)$$

$$W(r(t_i, n)) = \arctan \left(\frac{r(t_i, n)}{k} \right), \quad (14)$$

where α and k are parameters with length dimensions. By substituting Eqs. (13) and (14), Eq. (12) can be written in a simpler form as Eq. (3). In the double-pulse scanning method, the moving direction was calculated for every double-pulse emission using double sensory information. In this case, Eq. (12) can be written as Eq. (4).

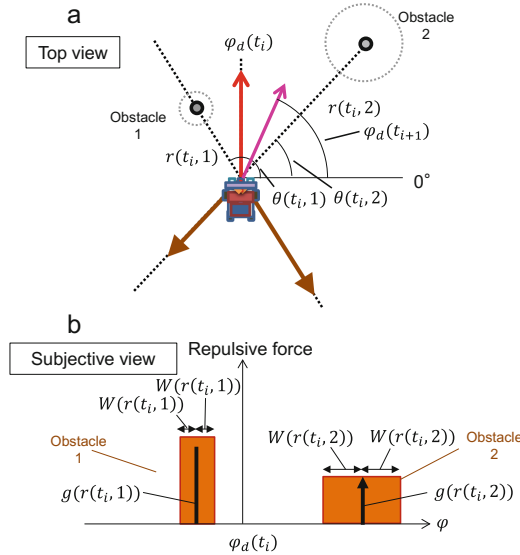


Fig. 10. Schematics of multi-obstacle-avoidance [MOA] model for obstacle avoidance. (a, b) Top and subjective views of the schematics of the MOA, respectively. The new moving direction $\varphi_d(t_{i+1})$ was determined according to the weighted sum of the vector of the current driving direction $\varphi_d(t_i)$ and imaginary repulsive force vectors arising from the recognized obstacles.

References

1. Barchi, J.R., Knowles, J.M., Simmons, J.A.: Spatial memory and stereotypy of flight paths by big brown bats in cluttered surroundings. *J. Exp. Biol.* **216**, 1053–1063 (2013)
2. Griffin, D.R.: *Listening in the dark: the acoustic orientation of bats and men* (1958)
3. Jen, P.H.-S., Kamada, T.: Analysis of orientation signals emitted by the CF-FM bat, *Pteronotus p. parnellii* and the FM bat, *Eptesicus fuscus* during avoidance of moving and stationary obstacles. *J. Comp. Physiol.* **148**, 389–398 (1982)
4. Surlykke, A., Ghose, K., Moss, C.F.: Acoustic scanning of natural scenes by echolocation in the big brown bat, *Eptesicus fuscus*. *J. Exp. Biol.* **212**, 1011–1020 (2009)
5. Iida, F.: Cheap design approach to adaptive behavior: walking and sensing through body dynamics. In: *Proceedings of AMAM 2005*, p. 15 (2005)
6. Pfeifer, R., Lambrinos, D.: Cheap vision—exploiting ecological niche and morphology. In: Hlaváč, V., Jeffery, K.G., Wiedermann, J. (eds.) *SOFSEM 2000. LNCS*, vol. 1963, pp. 202–226. Springer, Heidelberg (2000). https://doi.org/10.1007/3-540-44411-4_13
7. Dear, S.P., Simmons, J.A., Fritz, J.: A possible neuronal basis for representation of acoustic scenes in auditory cortex of the big brown bat. *Nature* **364**, 620–623 (1993)

8. Suga, N.: Amplitude spectrum representation in the Doppler-shifted-CF processing area of the auditory cortex of the mustache bat. *Science* **196**, 64–67 (1977)
9. Geipel, I., Jung, K., Kalko, E.K.: Perception of silent and motionless prey on vegetation by echolocation in the gleaning bat *Micronycteris microtis*. In: *Proceedings of the Royal Society B*, p. 20122830 (2013)
10. Aihara, I., Yamada, Y., Fujioka, E., Hiryu, S.: Nonlinear dynamics in free flight of an echolocating bat. *Nonlinear Theory Appl. IEICE* **6**, 313–328 (2015)
11. Fujioka, E., Aihara, I., Watanabe, S., Sumiya, M., Hiryu, S., Simmons, J.A., et al.: Rapid shifts of sonar attention by *Pipistrellus abramus* during natural hunting for multiple prey. *J. Acoust. Soc. Am.* **136**, 3389–3400 (2014)
12. Ghose, K., Horiuchi, T.K., Krishnaprasad, P.S., Moss, C.F.: Echolocating bats use a nearly time-optimal strategy to intercept prey. *PLoS Biol.* **4**, e108 (2006)
13. Ghose, K., Moss, C.F.: The sonar beam pattern of a flying bat as it tracks tethered insects. *J. Acoust. Soc. Am.* **114**, 1120–1131 (2003)
14. Ghose, K., Moss, C.F.: Steering by hearing: a bat’s acoustic gaze is linked to its flight motor output by a delayed, adaptive linear law. *J. Neurosci.* **26**, 1704–1710 (2006)
15. Yamada, Y., Hiryu, S., Watanabe, Y.: Species-specific control of acoustic gaze by echolocating bats, *Rhinolophus ferrumequinum nippon* and *Pipistrellus abramus*, during flight. *J. Comp. Physiol. A* **202**, 791–801 (2016)
16. Kothari, N.B., Wohlgenuth, M.J., Hulgard, K., Surlykke, A., Moss, C.F.: Timing matters: sonar call groups facilitate target localization in bats. *Front. Physiol.* **5**, 168 (2014)
17. Moss, C.F., Bohn, K., Gilkenson, H., Surlykke, A.: Active listening for spatial orientation in a complex auditory scene. *PLoS Biol.* **4**, e79 (2006)
18. Warnecke, M., Lee, W.-J., Krishnan, A., Moss, C.F.: Dynamic echo information guides flight in the big brown bat. *Front. Behav. Neurosci.* **10**, 81 (2016)
19. Moss, C.F., Surlykke, A.: Probing the natural scene by echolocation in bats. *Front. Behav. Neurosci.* **4**, 33 (2010)
20. Vanderelst, D., Holderied, M.W., Peremans, H.: Sensorimotor model of obstacle avoidance in echolocating bats. *PLoS Comput. Biol.* **11**, e1004484 (2015)
21. Seara, J.F., Strobl, K.H., Schmidt, G.: Path-dependent gaze control for obstacle avoidance in vision guided humanoid walking. In: *Robotics and Automation*, pp. 887–892 (2003)
22. Eckmeier, D., Geurten, B.R., Kress, D., Mertes, M., Kern, R., Egelhaaf, M., et al.: Gaze strategy in the free flying zebra finch (*Taeniopygia guttata*). *PLoS One* **3**, e3956 (2008)
23. Land, M.F., Collett, T.: Chasing behaviour of houseflies (*Fannia canicularis*). *J. Comp. Physiol.* **89**, 331–357 (1974)
24. Land, M.F., Lee, D.N.: Where we look when we steer. *Nature* **369**, 742–744 (1994)